MEASUREMENT OF (γ, p) REACTIONS WITH $\Delta E - E$ TELESCOPE AT MAX-LAB FACILITY

D. Burdeinyi[1], **J. Brudvik**[2], **V. Ganenko**[1], **K. Hansen**[3], **K. Fissum**[3], **L. Isaksson**[3], **K. Livingston**[4], **M. Lundin**[2], **B. Nilsson**[2], **B. Schröder**[2,3]

[1] *National Science Center "Kharkov Institute of Physics and Technology", Kharkov, Ukraine;*

[2] *MAX-lab, Lund University, SE-221 00 Lund, Sweden;*

[3] *Department of Physics, Lund University, SE-221 00 Lund, Sweden;*

[4] *Department of Physics and Astronomy, University of Glasgow, Glasgow G12 8QQ, Scotland, UK*

The paper considers the results of experiments on the reactions $^{12}C(\gamma, p)^{11}B$ and $d(\gamma, p)n$ in the energy range of tagged photons 35...80 MeV. Demonstrated the possibility identification of protons by $\Delta E - E$ using CsI/SSD telescope. Using the spectra of the missing energy defined the values of differential cross sections of these reactions in the range of photon energies. The good agreement of the experimental results with the available data in the literature.

PACS: 03.65.Pm, 03.65.Ge, 61.80.Mk

1. INTRODUCTION

The (γ, p) reactions are of the most studied photonuclear processes, which have been widely investigated in the energy range between the Giant Dipole Resonance and the pion production threshold, see [1] and reference in their. The purpose of these researches was, on the one hand, to study nuclear structure, and on the other hand, to determine the mechanisms of photon absorption by nuclei in this energy range, in particular, to study relative role of the direct knock-out and quasi-deuteron mechanisms. Production of linearly polarized photon beam at MAX-lab [2] opened a new possibility for investigations.

One of a simple experimental technique, available in the MAX-lab at present time and which could be applied for the (γ, p) reactions investigations is a ΔE-E CsI/SSD telescope [3]. The telescope consists of two single-sided silicon strip detectors and CsI counter which function as $(\Delta$E) and (E) detectors, respectively. In order to study the telescope characteristics, and its experimental possibility of the (γ, p) reactions identification, the measurements of a deuteron and a carbon photodisintegration have been performed. In this paper results of the data processing are presented, and methods of the (γ, p) reactions selection are analyzed.

2. EXPERIMENTAL APPARATUS AND TECHNIQUE

The measurements have been produced at the MAX-lab nuclear physics facility, described in [4] in detail. The facility has advanced infrastructure for precision photonuclear experiments in energy range from Giant Dipole Resonance and to some ten MeV above the pion threshold: (i) The electron beam with maximal energy $E_0 \approx 200$ MeV, duty cycle $df \approx 50...70\%$ and current up to 20 nA; (ii) Two tagging systems which cover energy interval from 10 to 180 MeV with energy resolution 0.5...1 MeV; (iii) Systems of the beam diagnostic and control.

2.1. Beam and beam line

The electron beam was extracted from the MAX-I storage ring which worked in a stretcher mode. Injection of electrons into the ring was performed by a double-section linear accelerator at a frequency of 10 Hz and duration of the injected electron pulse about 200 ns. The electron energy was $E_0 = 192.7$ MeV. The electrons were slowly extracted from the MAX-I ring during 100 ms and by a beam transportation system delivered into experimental hall.

A schematic picture of the beam line and experimental set up is shown in Fig.1. A dipole magnet (1) directed the electron beam towards 50 μm Al photon radiator fixed in a target holder of a goniometer (5). The goniometer was placed in a vacuum chamber between magnets of the end-point tagger (ET) (4) and the main tagger (MT) (6). The electron current on photon radiators was $\sim 5...10$ nA. The beam size on the radiators was no more than 2 mm. A non-interacting part of the electron beam was deflected to the beam dump (8) by the MT magnet, where it was absorbed by a Faraday cup. At the MT magnet setting, used in the experiment, the electrons passed a section of air (~ 135 cm) and two steal foils 25 μm thick on its way to the beam dump [4].

A photon collimator was placed on the distance 2140 mm from the photon radiators, before the shielding wall. The collimator total length is 40 cm. It consists of heavy metal main collimator 108.5 mm long with the variable entrance openings followed by a scrubber magnet ~ 100 mm long, and a scrubber collimator 200 mm long. The 12 mm opening was used in the measurements.
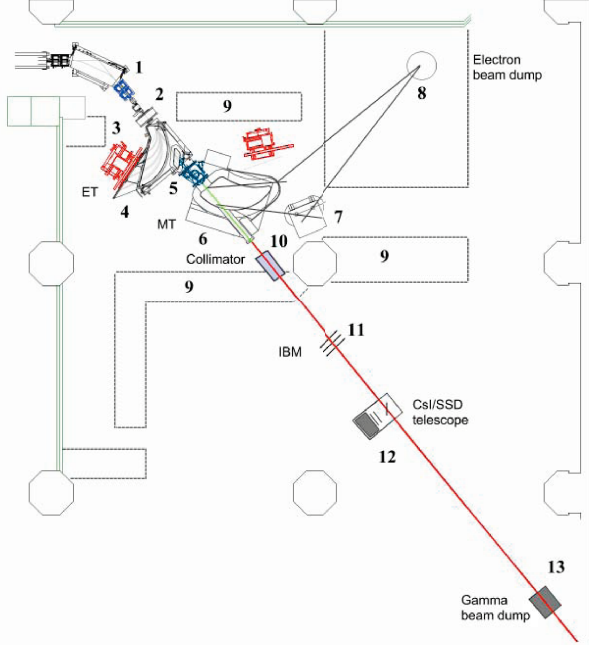
Fig.1. *Scheme of the MAX-lab beam line for photonuclear researches. 1-bending magnet (50^0); 2-vertical and horizontal steering magnets; 3-photon radiator for end-point tagger; 4-end-point tagger (ET); 5-goniometer; 6-main tagger (MT); 7-additional dump magnet; 8-Faraday cup; 9-shielding; 10-photon collimator; 11-gamma monitor (IBM); 12-SSD/CsI telescope; 13-photon beam dump*

It provided the collimation angle $\theta_c \approx 1.2\theta_\gamma$ for a point-like electron beam ($\theta_\gamma = m_e c^2/E_0$ is the characteristic angle of bremsstrahlung, E_0 and m_e are the electron energy and mass). The intensity of the photon beam was controlled by a scintillation gamma beam monitor (IBM) (11) [4].

2.2. Photon beam tagging system

The bremsstrahlung spectrum, generated due to interaction of high energy electrons with a photon radiator, contains energies from zero to maximal electron energy E_0. The photon energy value is obtained from the relation $E_\gamma = E_0 - E'_e$, where E'_e is the energy of a post-bremsstrahlung electron. The post-bremsstrahlung electrons are detected by a focal plane (FP) hodoscope, placed along the MT magnet focal plane. Their energy is determined by the MT magnet field and position of the counters of the FP hodoscope along the focal plane. In our case the focal plane position was different from the standard location due to upstream shift of the position of the pho-

ton radiators, fixed in the goniometer target holder. The new focal plane position was calculated by tracing electrons in the magnetic field of MT and presented in [4].

The FP hodoscope consists of two rows of scintillators 25 mm wide and 3.2 mm thick. The first row, facing the exit window of the MT, contains 31 and the second row, behind the first, contains 32 scintillators. The overlap between scintillators of the rows was 50%. The coincidence requirement to overlapping scintillators resulted in 62 channels for detecting the post-bremsstrahlung electrons.

The momentum acceptance of the MT spectrometer is $\pm 40\%$ of P_C, where P_C is the central momentum of the MT tagging spectrometer. Its value is determined in [4]. In our beam run, in order to extend the tagging interval to lower photon energies, the hodoscope was shifted above the position corresponding to momentum acceptance $+40\%$, so that the energy interval above the $+40\%$ mark was included. It covered the tagger channels 50-62, corresponding to energies $E_\gamma = 21.9...33.8$ MeV. Thus, the total tagged energy range of the photon beam tagging was $E_\gamma = 21.9...78.8$ MeV.

Energy resolution of the tagger system in the case of coincidence requirement between the scintillator rows depends on the dispersion of the MT magnet (presented in [4]), the effective width of the tagging channel along the focal plane, which depends on overlap of the scintillators, and an angle between the direction of the post-bremsstrahlung electron trajectories and the MT focal plane. The energy resolution of the tagged photon channels was calculated for 50% overlap and normal incident of the scattered electrons to the MT focal plane. The resolution smoothly varies from $\Delta E_\gamma \approx 0.8$ MeV, for the high end of the tagged range, to $\Delta E_\gamma \approx 1$ MeV at $E_\gamma \approx 38$ MeV, and then it is almost constant in the interval $E_\gamma = 22...38$ MeV. However, the real angle between the direction of the post-bremsstrahlung electron trajectories and the new MT focal plane is 52.6^0. This results in a difference between the momentum acceptance of odd and even FP channels, when coincidence requirement is applied to the overlapping scintillators. This brings to different rate of the post-bremsstrahlung electrons detected by the FP channels. To exclude this effect, summation of the yields over neighboring FP channels was produces.

2.3. Targets

The measurements have been carried out using a CD_2 and a CH_2 targets. The CH_2 target was applied both for carbon disintegration measurement and for removing the background contribution from this process to the deuteron disintegration. The CD_2 target had a disc shape, 75 mm in diameter and 1 mm thick. The CH_2 target had a square form, $150.2 \times 150.2\,mm^2$ and 1.1 mm thick. The density of the targets was determined by their weighing and calculation their volume. The calculated density of

the CD_2 target was $\rho = 1.026\,g/cm^3$, and the CH_2 target $\rho = 0.937\,g/cm^3$.

The targets were positioned on the distance $\approx 2\,m$ from the photon collimator under angle $\theta_m = 60^0$ to the photon beam direction. The effective number of deuteron per area was $N_D = 1.541 \times 10^{22}\,cm^{-2}$, and the effective number of ^{12}C nuclei per area was $N_C = 0.771 \times 10^{22}\,cm^{-2}$ for the CD_2 target and $N_C = 0.885 \times 10^{22}\,cm^{-2}$ for the CH_2 target.

2.4. CsI/SSD telescope

The emitted protons were detected by a CsI/SSD telescope [3], schematically shown in Fig.2. The telescope consists of two identical single-sided silicon strip detectors (SSDs), and a CsI(Tl) counter. The SSD detectors (ΔE) are of octagonal shape, have an active area $3300\,mm^2$ and a thickness 0.5 mm. They have 64 strips, each with a width of 1 mm. The strips are paralleled in groups of two for the read-out, thus yielding an effective strip width of 2 mm. The active aria of the detectors was wrapped Al foil 15 μm thick. The CsI(Tl) detector (E) is of a cylinder shape 12.5 cm in diameter and 10 cm long, placed in Al container with the standard Al-front-foil.
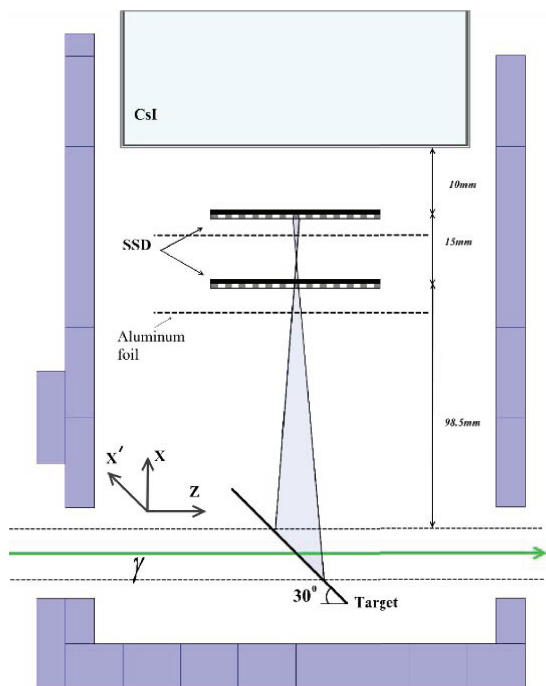
Fig.2. *Scheme of the CsI/SSD telescope, see text*

The telescope was placed under angle $\theta_p = 90^0$ to the beam axis. The distance between the first SSD and the center of the photon beam sport on the target was 98.5 mm, the distance between the SSDs was 15 mm, and the distance between the second SSD and CsI was 10 mm.

## 3. DATA ANALYSIS

The measurements have been carried out in the course of three short (~ 1 hour) beam runs for both

targets. The total duration of the data taking was ~ 3.52 hour for the CD_2 and ~ 2.92 hour for the CH_2 targets.

3.1. Proton identification

Proton identification has been performed by standard $\Delta E - E$ method, based on relationship between the energy losses in a ΔE detector and full energy E of the particles with different masses. Typical two-dimensional plot pairs of ADC signals from the SSD (ΔE) and CsI (E) detectors is shown in Fig.3, where one can see separation of the protons from other particles (electrons, deuterons, etc.) into clear band. For further analysis the background particles were removed by special soft cut of the $\Delta E - E$ plot, shown in Fig.3. The selected proton yield results from various reactions of the carbon disintegration, and the deuteron disintegration, as well, if the CD_2 target is used. At that, for photon energies $E_\gamma < 52\,MeV$, due to threshold of the proton detection by the telescope, only two-body reactions of the carbon disintegration, $^{12}C(\gamma, p)^{11}B$, give contribution to the proton yield, in which the residual nucleus is in the ground state or one of the low-lying excited states with excitation energies $E_{ex} = 2.13, 5.02, 6.74, 6.79$ and $7.29\,MeV$. At higher photon energies, there is some contribution from the processes with higher exited states of ^{11}B and two-nucleon emission.
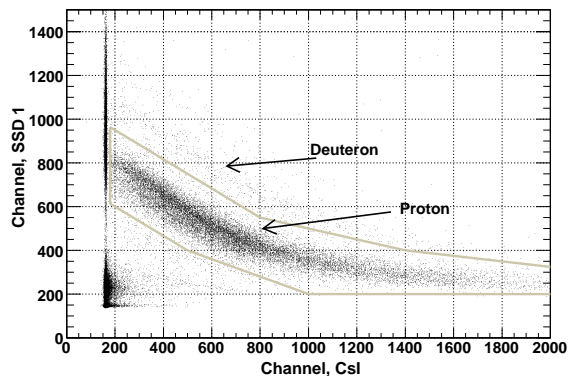

Fig.3. *Two-dimensional plot pairs of corresponding signals from the SSD and CsI detectors. Lines demonstrate separation of the proton band by special soft cut*

3.2. Time coincidence focal plane hodoscope detectors with CsI/SSD telescope

The stretched electron beam at MAX-lab has a rather complicated time structure which complicates the search for coincidences between the FP detectors and the CsI/SSD telescope signals. The CsI/SSD telescope (the coincidences between the SSDs and the CsI detector) produces trigger signals, which are generated by protons, electrons and other background particles, and electronic noise. Their number is identified by a selfcoincidence in the CsI/SSD trigger TDC. The trigger signals start all time TDCs of the FP array which are stopped by the pulses from the

FP detectors. Thus, the first step in the analysis consists of selecting events triggered by the CsI/SSD telescope, corresponding to the proton band, Fig.3. After such selection the random coincidences contribution in the FPtdc spectrum was strongly decreased.

The trigger start timing was determined by the OR of the SSDs signals. These SSD signals came from leading edge discriminators, and thus they had a significant time walk ($\sim 20\,$ns). As a result, the time coincidence FPtdc spectra were spread and there was no clear peak of the time coincidence. In order to cancel this time walk, the CsI detector was used as a time reference, i.e., the CsI TDC was subtracted from all other TDCs, taking the different TDC conversion gains into account. In this case only events above the CsI discriminator threshold were used. Having performed the steps outlined above, coincidence peak appears in the individual tagger TDCs, as shown in Fig.4, where one can see a strong prompt peak of the time coincidence of the FP and CsI/SSD telescope signals on top of random background. The time resolution of the FPtdc coincidence is $\approx 2...3\,$ns.
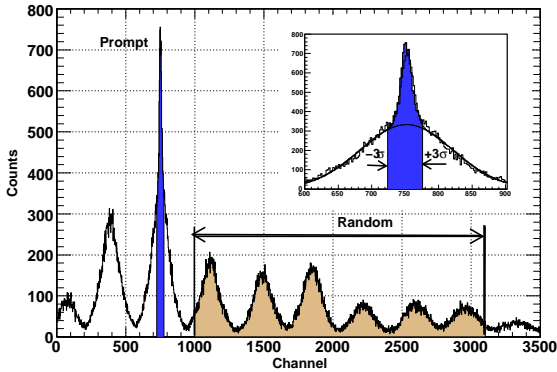
Fig.4. *The time coincidence spectra (FPtdc) between the SSD/CsI telescope and the FP channel, corresponding to photon energy* $E_\gamma = 50.4 \pm 0.5\,MeV$, *after selecting events from the proton band, and cancellation the SSD signals time walk. Blue color shows the prompt peak range, brown color shows range of the random coincidence which is used for the background spectrum construction. Curves in insertion are Gauss fits of the background and the prompt peak, see text*

Due to slightly varying delays for the tagger signals, the prompt peaks will not be in exactly the same position for each TDC channel but can be differed up to several tens of the TDC channels. In order to enable summing the FPtdc spectra, the prompt peaks for all FP channels were shifted to identical position. In order to produce the shift, the coordinates of the peak's positions were determined for all FP channels. For that the time structure of the random background under the prompt peak of the FPtdc spectrum was described by approximating the distribution with a Gaussian, Fig.4. Then the whole spectrum was fitted with a sum of two Gaussians: a broad Gaussian approximating the background under the peak, and

a narrow Gaussian describing the coincidence peak. From the fit the position μ and the standard deviation σ of the peak were determined. The range $\mu \pm 3\sigma$ was used to define the prompt region, shown blue shaded in Fig.4. Having the prompt peaks coordinates for all FP channels, the prompt peaks in all spectra were shifted to the same 750 channel of the FPtdc.

In the prompt region, $\mu \pm 3\sigma$, there are two types of events: true coincidence events (from a deuteron and various channels of carbon disintegration, an electromagnetic background), and random events. The region to the right of the peak, shown brown shaded in Fig.4, where only random events are presented, are subsequently labeled as the random region. Using the prompt and random region so defined, two different missing energy spectra can be generated: the spectrum for events in the prompt region, and one for events in the random region.

3.3. Tagging efficiency

A large portion of the tagged-photon beam was collimated away, thus not every electron registered in the focal plane detectors corresponded to a photon incident on the target. This loss is given by the photon beam tagging efficiency, which relates the number of photons, impinging on the target, e.g., corresponding to the tagger channel (i), $N_{\gamma,ch}(i)$, to the number of post-bremsstrahlung electrons, detected by the focal-plane array channel (i), $N'_e(i)$,

$$\varepsilon_{tag}(i) = \frac{N_{\gamma,ch}(i)}{N'_e(i)}. \tag{1}$$
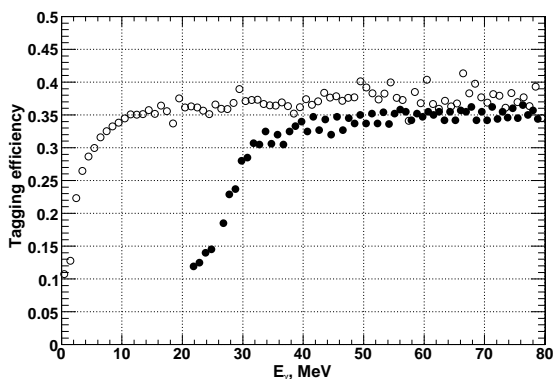
Measurements of the tagging efficiency are usually performed at strongly reduced the electron beam current by a special detector, placing in the photon beam path, which detects all photons that passed through the collimator. In our case the tagging efficiency was measured with a NaI detector $25 \times 25 \times 25\,cm^3$ [5]. The number of photons $N_{\gamma,ch}(i)$ was determined from ADC spectrum of the NaI signals, taking into account only the part, corresponding to the tagged photon interval. The numbers of electrons, recorded in the focal plane detectors $N_{FP}(i)$, were determined using the TDCs spectra, in which "self-coincidence" peaks were generated by the electrons, registered by the FP hodoscope counters. The peaks include also background contributions,

$$N_{FP}(i) = N'_e(i) + N_{bg,beam}(i) + N_{bg,const}(i), \tag{2}$$

$N_{bg,beam}(i)$ is the background yield generated by the beam and detected by the i-th FP counter. This background may come from various sources, including Meller electrons from the radiator and the beam halo striking a vacuum chamber. The $N'_e(i)$ and $N_{bg,beam}(i)$ rates are proportional to the beam intensity. $N_{bg,const}(i)$ is the background resulting from a constant room background (cosmic radiation, activation), which does not depend on the beam intensity.

The measured tagging efficiency is no usually corrected for the beam-related background. On the one

hand, it is no possible to determine correctly the real background value, because there is no monitor of the beam intensity when the radiator is removed from the low-intensity electron beam, while the intensity may vary significantly over a run. Furthermore, removing the radiator one may change the background situation, e.g., with the radiator-in measurements, the residual electrons from the low-energy part of the bremsstrahlung spectrum may hit the beam pipe on their way to the dump, and this background is not present, as well as the Meller electrons, when the radiator is removed. On the second hand, because this background presents in the same proportion in the low and high intensity runs, one may relate the number of photons with sum value $N'_e(i) + N_{bg,beam}(i)$. Besides, the high intensity radiator-off measurements demonstrated that this background contribution was usually no more than 1...2%.

Fig.5. _Tagging efficiency, measured (full circles) and simulated (empty circles), as a function of photon energy, corresponding to the focal-plane channels. See text for details_

Thus, correction of the tagging efficiency only on the constant room background contribution was produced. The average value of this background was determined in the beam-off measurements and was $n_b \sim 0.1\,Hz$ for all focal-plane channels, so at high beam intensity this background count rate was negligible on comparison with the count rates of the residual electrons and the background generated by the beam. However, at low intensity, being at the tagging efficiency measurement, the room background contribution can reach $\sim 2...3\%$, and should be taken into account. Thus, the tagging efficiency ε_{tag} is given by (see [6] for details)

$$\varepsilon_{tag}(i) = \frac{N_{\gamma,ch}(i)}{N_{FP}(i) + t_{liv}n_b}, \qquad (3)$$

where t_{liv} is the live time during the tagging efficiency measurement. The results of the tagging efficiency measurements are presented in [5] and shown in Fig.5. The tagging efficiency is weakly decreased at photon energy decreasing in the interval $E_\gamma \approx 40...80\,MeV$, then it steeply decreases for energies $E_\gamma < 40\,MeV$. Such behavior may be due to increasing the background contribution to the FP rate, small at the high

energies and strongly increasing at $E_\gamma < 40\,MeV$. Value of the measured tagging efficiency, averaged over $E_\gamma \approx 50...80\,MeV$ is $\varepsilon_{tag} = 0.350 \pm 0.002$.

3.4. Energy calibration and solid angle of the telescope

Because of large elliptic beam sport on the target, small distance between the target and the telescope, various materials on the proton way, there no simple analytical expressions for determination the proton energy losses, angular capture, and effective solid angle of the telescope. Thus, a Monte Carlo simulation of the setup was performed using the GEANT-4 software package [7]. Three associated blocks of the modeling were realized: (i) Simulation of interaction of an electron beam with a photon radiator, and the emitted photon passing through photon collimator; (ii) Simulation of passing of the protons, produced in the target, through the CsI/SSD telescope, and calculation their energy losses; (iii) Determination of the telescope angular capture and the solid angle.

#### 3.4.1. Simulation of electron beam interaction with a radiator

Simulation began with modeling interaction of the electron beam with energy of $E_0 = 192.7\,MeV$ with an aluminium photon radiator of $50\,\mu m$ thick. The interaction points of the electrons with the radiator were randomly distributed within the electron beam spot on the radiator, of $0.9 \times 2.2\,mm^2$ in vertical and horizontal directions, respectively. Momenta of the bremsstrahlung photon and the post-bremsstrahlung electron were obtained from the simulation of the bremsstrahlung process with the GEANT-4 package code. Then it was checked, firstly, if the photon passed the photon collimator, described above, having an aperture of $12\,mm$ in diameter, and, secondly, if the post-bremsstrahlung electron exited from the MT magnet. It can be under condition that vertical displacement of the post-bremsstrahlung electron on its way in the magnet chamber was less the vertical size of the magnet chamber ($\pm 75\,mm$ from the middle plane).

The numbers and energies of the simulated initial electrons (N_e) and secondary particles - the post-bremsstrahlung electrons ($N'_{e,mc}$), which passed the MT magnet chamber, the emitted bremsstrahlung photons ($N_{\gamma,tot}$) and the photons, which passed the photon collimator ($N_{\gamma,mc}$), were fixed. Then the secondary particles were sorted on the energy bins, corresponding to the FP channels energy and width. The accumulated data base allows one to calculate the photon beam intensity distribution on the target and calculate the tagging efficiency,

$$\varepsilon_{tag,m}(i) = \frac{N_{\gamma,hit}(i)}{N'_{e,m}(i)}. \qquad (4)$$

The simulated tagging efficiency is shown in Fig.5. It is practically constant in the range $E_\gamma = 40...80\,MeV$, the average value in this interval is

$\varepsilon_{tag,m} = 0.374 \pm 0.002$ that is $\sim 6.8\%$ more than the experimental value. The difference may be due to the beam dependent background contribution to the FP detectors counting rate. The estimation of this background contribution can be made by relation $f_{bg} = 1 - \varepsilon_{tag}/\varepsilon_{tag,m}$, which give the value $f_{bg} = 0.06$ in the range $E_\gamma = 40...80\,\mathrm{MeV}$. This estimation is close to the approximate experimental estimation of the background, $\sim 1...3\%$, obtained usually in the radiator-off measurements (see note above).
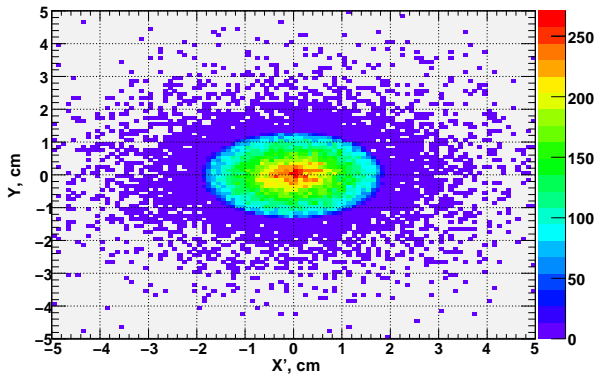
Fig.6. *Two-dimensional distribution of the photon beam intensity (shown by color scheme) on the target*

Results of the measurements and the simulation have shown that $\sim 35\%$ photons passed the collimator and hit the target. The calculated beam spot size on the target is shown in Fig.6. It is $\sim 13.8\,\mathrm{mm}$ (FWHM) in vertical, and $28.1\,\mathrm{mm}$ in horizontal planes, respectively. Large size of the beam spot increased the telescope angular capture and worsened its angular resolution.
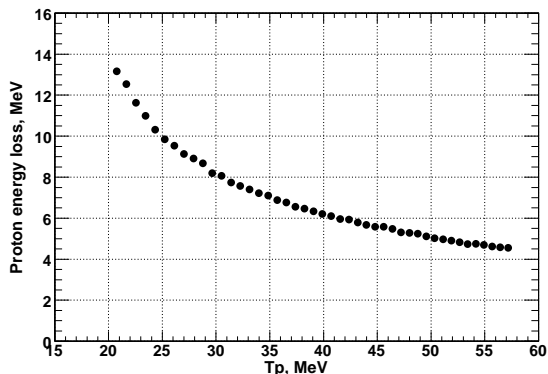
3.4.2. Proton energy losses

On the second stage, the simulation of the proton passing through the CsI/SSD telescope was produced, and the proton energy losses on this way were calculated. Because the target was thin, one can consider the horizontal and vertical coordinates (X,Y) of the photon hit of the target, as coordinates of the photon interaction point with the target nucleus. Distribution of these points within the beam spot is proportional to the photon beam intensity distribution. The third coordinate (Z) was played randomly along the photon trajectory across the target. Array of all these interaction points determined active volume of the target.

Energy of protons emitted from the interaction point was calculated using the reaction kinematics, $d(\gamma,p)n$ or $^{12}C(\gamma,p_0)^{11}B$, and values of the photon energy and polar angle of the proton emission. The photon energy values were obtained on the previous stage of the bremsstrahlung simulation, but on this stage only energies being within the tagged interval, $E_\gamma = 21.9...78.8\,\mathrm{MeV}$, were considered. The polar and azimuthal angles, defining direction of the proton emission, were played isotropic. The other parameters included in the simulation, describing the targets, geometry of the CsI/SSD telescope, and the matter on the protons way, have been partly indicated above in the sections 1.3 and 1.4, and the others are presented below:

- the target matter in which the protons pass distance from the interaction point to exit from the target;

- the air interval from the target to the first SSD detector, which depends on the exit point from the target and the point of the proton hitting into the SSD;

- two silicon strip detectors of hexagonal shape and of 0.5 mm thick;

- two Al foils, each of $15\,\mu m$ thick;

- two air intervals, of 15 mm between the first and the second SSDs, and of 10 mm between the second SSD and the CsI detector;

- the Al wall of the CsI box of 0.5 mm thick.

From all generated protons ($N_{p,tot}$), referred as "events", there were fixed those ($N_{p,det}$) which passed through the telescope within the active aria of the SSD detectors and entered into the CsI. Such protons were counted as detected ones. For these "events", there were fixed: initial conditions (location, momentum) in the point of origin, the energy losses in each materials, being on its way, energy deposited in the SSDs and CsI detectors, coordinates of the proton hits the SSD detectors, and points of entering into the CsI. The energies deposited by protons in the detectors and their energy losses in the materials were averaged over intervals of the emitted protons energies, corresponding to the energy width of the photon tagger channels. The calculated energy losses are shown in Fig.7, as a function of the initial proton energy (in the point of origin in the target).

Fig.7. *Proton energy losses on its way from the point of origin in the target to the CsI detector, averaged over intervals of the initial proton energies, corresponding to the photon energy resolution of the FP hodoscope*

The energy losses are $\Delta E_p \approx 7\,\mathrm{MeV}$ for protons with initial kinetic energy $T_p = 36\,\mathrm{MeV}$ and $\Delta E_p \approx 13\,\mathrm{MeV}$ for $T_p = 20\,\mathrm{MeV}$. The accuracy of the energy losses calculation is determined by the energy loss tables available through the GEANT-4 package,

which is believed to be within about 1...2%. Simulation has shown that threshold of the proton detection by the SSD/CsI telescope is $T_{th} \approx 18\,\text{MeV}$ that corresponds to the photon energy $E_\gamma \approx 40\,\text{MeV}$ for the $d(\gamma, p)n$, and $E_\gamma \approx 36\,\text{MeV}$ for the $^{12}C(\gamma, p_0)^{11}B$ reactions.

3.4.3. CsI detector energy calibration

Energy calibration assumes establishing a correlation between the pulse-height of the CsI detector signals and energy of the incoming protons.

The CsI pulse-height spectra, corresponding to the events from the prompt region of the Fptdc spectra, demonstrate two large maxima (if data from the CD_2 run is used) for all the FP channels energies. They correspond to the signals, produced by protons emitted from the $d(\gamma, p)$ (the first peak) and the $^{12}C(\gamma, p_0)^{11}B$ reactions, as one can see in Fig.8 (left). The maxima are on a smooth random background, resulted from the random FPtdc coincidences events, being under prompt peak.
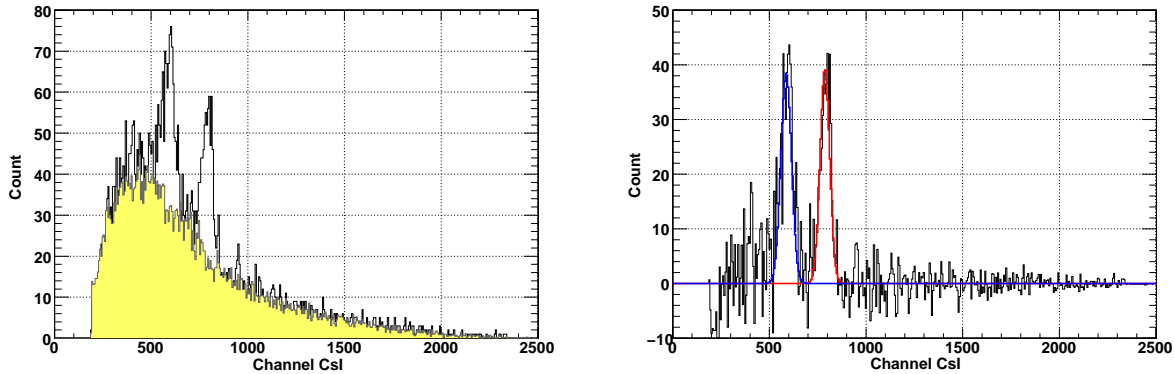
Fig.8. *Left: Pulse-height spectrum of the CsI detector signals, produced by protons emitted from the CD_2 target due to the $d(\gamma, p)$ and the $^{12}C(\gamma, p_0)^{11}B$ reactions. Photon energies are $E_\gamma = 50.4 \pm 0.5\,MeV$. Yellow histogram is the constructed background. Right: Pulse-height spectrum after background subtraction. Curves are the Gauss fits*

In order to determine exact position of the peaks, the background was subtracted. For that the background pulse-height spectrum was generated, using the events in the random region of the Fptdc spectrum.

Fig.9. *Relation between the pulse-height of the CsI detector signal (the ADC peak position) and: (i) Energy deposited by proton in the CsI detector (circles), average over results obtained for the $d(\gamma, p)$ and $^{12}C(\gamma, p_0)^{11}B$ reactions. Line is the linear fit; (ii) Energy of the initial proton, produced in the target (triangles). Line is the third degree polynomial fitting*

The background spectrum was normalized to the prompt one and subtracted, Fig.8 (right). The nor-

malization factor was determined coming from requirement of equality the number of events of the both spectra in the "background range", being on the right side of the peaks, e.g., above the 900-th channel in the Fig.8 (left). The maxima positions were determined by the fitting of the peaks by Gaussian.

Initial energy of the protons, producing the observed CsI pulse-height spectra, were calculated using the tagged photon energy value of the corresponding FP channel, and the polar angle value of the proton emission, $\theta_p = 90^0$. Taking into account the energy losses, the energy deposited by the proton into the CsI detector was determined. Thus, correlation between the deposited energy and the amplitude of the CsI detector signal (the ADC peak position) was obtained. Such correlations were obtained using proton emission from the $d(\gamma, p)$ and $^{12}C(\gamma, p_0)^{11}B$ reactions. They were, practically, identical. The average dependence is shown in Fig.9. It demonstrates linear dependence between the energy of incoming into the CsI proton and the detector CsI signal within energy interval $T_p = 10...50\,\text{MeV}$

For missing energy spectra construction, there is more appropriate the direct relation between the CsI detector pulse-height signal and initial energy of the proton, produced in the target. It is shown in Fig.9 by triangles. Due to increasing energy losses for low energy protons, there is deviation from linearity in the low energy range. This dependence was fitted

by third degree polynomial and was used for determination the initial proton energy at missing energy spectra construction.

3.4.4. Angular capture and effective solid angle

If not to use information about numbers of triggered strips in the first (n_1) and the second (n_2) silicon strip detectors, an angular aperture of the CsI/SSD telescope is determined by the size of active aria of the second SSD, its distance from the target, and the size of the target active volume.
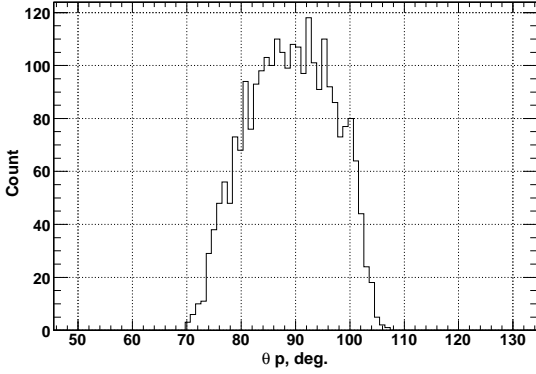
**Fig.10.** *Simulated angular capture of the SSD/CsI telescope*

The geometrical angular capture was calculated using the simulation data base, described above. The trajectories of the, so-cold, "detected protons", which were emitted from the target active volume, passed through the active aria of the both SSDs, and entered into the CsI, were constructed, and the corresponding polar angles of the particles emission were calculated
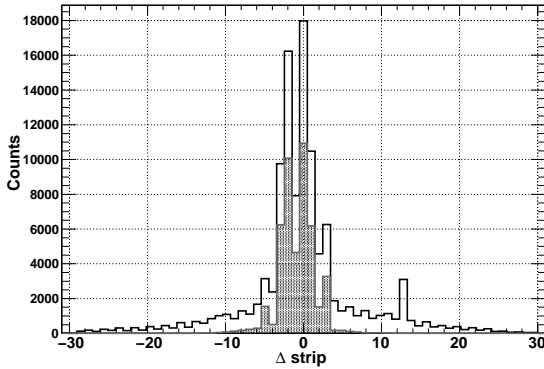
Fig.11. *Distribution of the number of events detected by the SSDs, as a function of difference, $\Delta = n_2 - n_1$, between numbers of triggered strips in the first (n_1) and the second (n_2) SSDs. The shaded histogram corresponds to events from the proton band in Fig.3*

The simulation has shown that in the case of detection of all particles, passing the active aria of the SSDs, the telescope angular capture is rather large, $\Delta\theta_p \approx 28^0$ (FWHM), and the telescope can detect

protons, emitted from the target, within the polar angles interval $\theta_p \approx 70^0...105^0$, as shown in Fig.10. At the distance between the first and the second SSD of 15 mm, the angular interval of the proton registration $\theta_p \approx \pm 20^0$ restricts the maximal difference between the triggered strip numbers in the SSDs, $\Delta = n_2 - n_1$, by value $\mid \Delta \mid \leq 3$, at that main bulk of the detected events should be within $\mid \Delta \mid \leq 2$ for FWHM telescope angular capture $\Delta\theta_p \approx 30^0$. The experimental distribution of the number of events, detected by the SSDs, as a function of the difference, $\Delta = n_2 - n_1$, is shown in Fig.11. One can see that there are practically no events with $\mid \Delta \mid \geq 3$ if the detected particles were taken from the proton band. The events with more difference are the background events, and their amount is negligibly small. The main bulk of the detected events are within $\mid \Delta \mid \leq 2$.
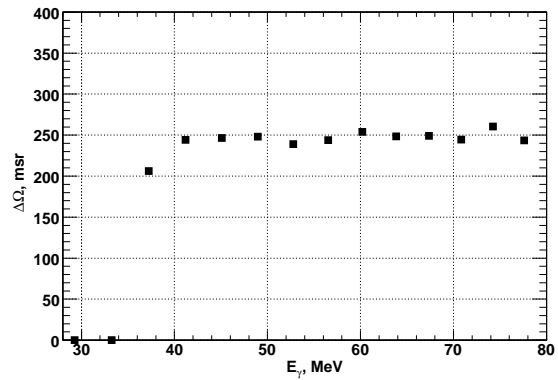
Fig.12. *The effective solid angle, as a function of tagged photon energy values, corresponding to the focal plane channels*

In order to increase statistics for further analysis, summation of the experimental data was produced for four physically adjacent FP channels. As a result, the FPtdc spectra were formed for twelve energy bins with central energies $E_{\gamma,bin}$ =37.2, 41.2, 45.1, 49.0, 52.8, 56.5, 60.2, 64.0, 67.4, 70.8, 74.2, 77.6 MeV, and the bin width $\Delta E_{\gamma,bin} \approx 4$ MeV. The effective solid angle of the telescope was calculated for all bins, using total numbers of the "generated", $N_{p,tot}(j)$, and the "detected protons", $N_{p,det}(j)$, from the data base,

$$\Delta\Omega(j) = 4\pi \frac{N_{p,det}(j)}{N_{p,tot}(j)} . \qquad (5)$$

The solid angle values are shown in Fig.12, as a function of the photon bin energy. The statistical uncertainty was calculated by,

$$\sigma(j) = \Delta\Omega \sqrt{\left(\frac{1}{N_{det}(j)} + \frac{1}{N_{tot}(j)}\right)} \qquad (6)$$

and was $\sim 2.6\%$ for all bins. The solid angle within the statistical accuracy is, practically, constant in the energy range $E_\gamma = 40...80$ MeV, its averaged value in this interval is

$$\Delta\Omega = 249.0 \pm 2.25 \, msr. \qquad (7)$$

The steep decrease at photon energies less 40 MeV is due to threshold of the proton registration.

As a check, the simulation was performed for a point source, for which the solid angle value $\Delta\Omega_p = 237.5\,msr$ was obtained. The analytical calculation performed for rectangle detector of the same square gave the solid angle value $240.9\,sr$, that is 1.4% more. The difference can be due to a different shape of the detectors. The systematic uncertainty due to uncertainties of the measurements of the set-up dimensions is estimated to be $\sim 2\%$.

3.5. The reactions selection

3.5.1. The $d(\gamma,p)n$ reaction. Mission energy spectra

There are two types of events in the prompt peak region, $\mu \pm 3\sigma$, of the FPtdc spectrum: true coincidences from various channels of the carbon disintegration (the deuteron disintegration, as well, if the CD_2 target is used), and the random background events. In order to separate contributions from the background and to select yield of the $d(\gamma,p)n$ and $^{12}C(\gamma,p)^{11}B$ reactions, a missing energy (MisE) method was applied. It assumes construction missing energy spectra of the reaction under study. The missing energy is given by the relation,

$$E_m = E_\gamma - T_p - T_r, \qquad (8)$$

where E_m is the photon energy, T_p is the proton kinetic energy, measured by the CsI detector and corrected to the energy losses on its way from the origin point to the detector, T_r is the energy of a recoil nucleus (neutron or ^{11}B) which is calculated using the reaction kinematics, known photon energy, and the proton emission angle value $\theta_p = 90^0$. Taking events from the prompt region of the FPtdc spectra, the prompt missing energy spectra were generated for all eleven energy bins for the CD_2 and CH_2 targets data.
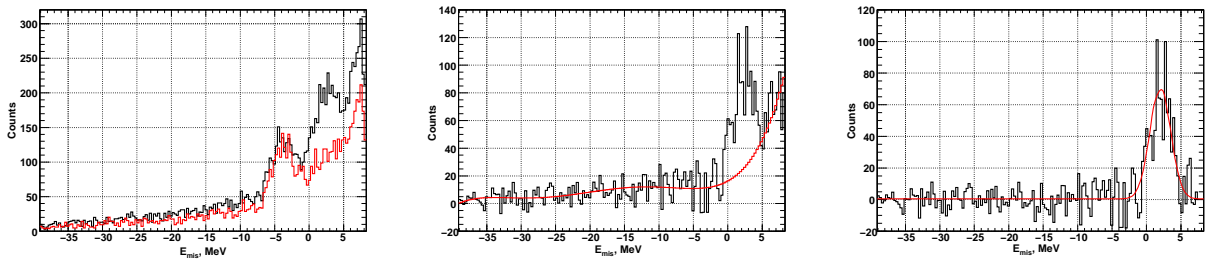
Fig.13. Left: missing energy spectra of the protons detected from the CD_2 (black line) and CH_2 targets after normalization (red line). Middle: the missing energy spectrum of the protons after subtraction the normalized CH_2 spectrum. Line is the five order polynomial fit the remaining background. Right: the missing energy spectrum of the $d(\gamma,p)n$ reaction after the background subtraction. Photon energy $E_\gamma = 49.0 \pm 2.0\,MeV$. The width of the histogram bin is $0.3\,MeV$

The spectra obtained from the CH_2 target data were normalized to experimental conditions, being at corresponding measurements with the CD_2 target. That is, the corrections were made to different photon flux and thickness of the targets, in order that yields of the carbon disintegration processes were identical for both targets, what is needed for subtraction the carbon disintegration background from the deuteron disintegration yield. As example, some MisE spectra are shown in Figs.13-15 (left). The recoil nucleus energy values were calculated for reaction of the deuteron disintegration, that is $T_r = T_n$. Shape of the presented spectra is typical for all bins: (i) There are maxima resulted from the reactions of a carbon and a deuteron (for measurements on the CD_2 target) disintegration, being on top of a random background; (ii) The background is distributed over a large range and decreased with the missing energy decreasing.
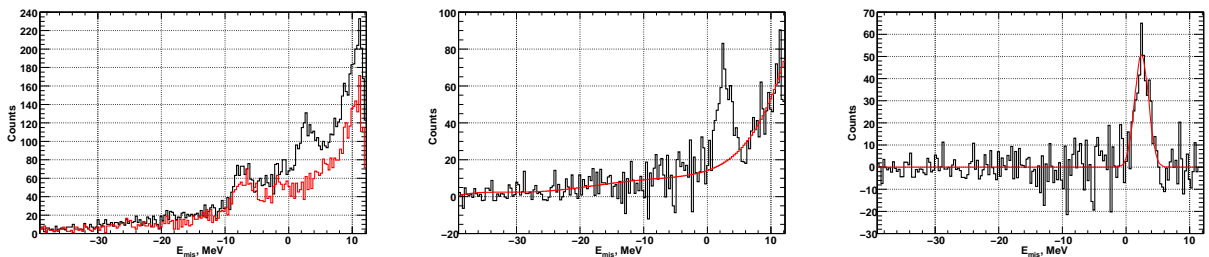
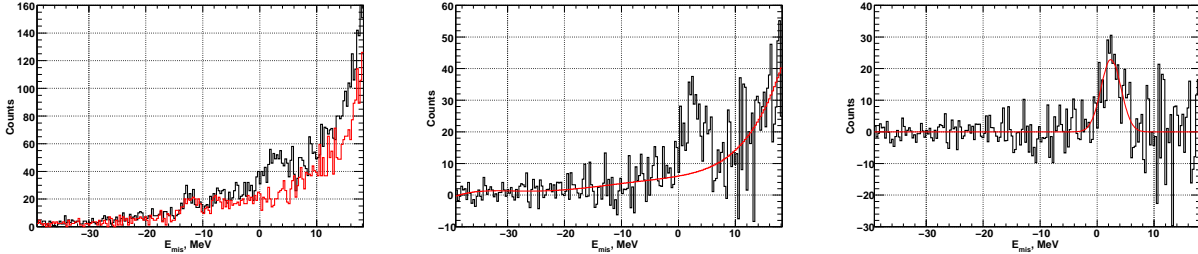**Fig.14.** The same for photon energy $E_{\gamma,bin} = 56.5 \pm 2.0\,MeV$

According to choice $T_r = T_n$, the events corresponding to reaction of the deuteron disintegration are located in a peak, position of which should be the same for all energy bins, and should be equal to the deuteron binding energy, $E_d \approx 2.2\,MeV$, that with a good accuracy is observed in the experiment, Figs.13-18.

There is a weaker maximum to the right side from the previous one. It can be seen more clearly in Figs. 16-18 (middle) for CH_2 target spectra after back-

ground subtraction. This peak corresponds to the sum of possible reactions $^{12}C(\gamma, p_{2-5})^{11}B$, when the nucleus ^{11}B is in one of higher excited states with $E_{ex} \sim 5.02$, 6.74, 6.79 and 7.29 MeV, which are also no separated owing to large energy resolution. The distance between the carbon and the deuteron max-

ima increases if the photon energy increases, and they are well separated in the CD_2 Emis spectra at photon energies $E_\gamma \geq 52$ MeV. For less energy the maxima corresponding to the above mention two-body carbon disintegration processes coincide with the deuteron peak.

Fig.15. *The same for photon energy* $E_{\gamma,bin} = 70.8 \pm 2.0\,MeV$

Effective way to remove all background contribution to the deuteron maximum, both from the carbon disintegration and random background, is to subtract the MisE spectra, measured on CH_2 target, from the spectra measured on CD_2 target after corresponding normalization. However, direct subtraction may give incorrect value of the $d(\gamma, p)n$ reaction yield because of the random background is not identical for CD_2 and CH_2 spectra. So, it is impossible to subtract simultaneously the random and carbon background correctly, thus, two-step procedure was applied. There were two variants of its application, different by execution sequence of the random and carbon background subtraction. In the first variant (Variant A), on the first step the carbon background was removed by subtraction of the normalized (as was described the above) CH_2 spectrum. The results of the subtraction are shown in Figs.13-15 (middle). One can see that the remaining random background is small in the left side of the spectrum, but it reaches $\sim 20\%$ under the deuteron peak and has non trivial energy dependence. On the second step, this remaining background, with the exception the deuteron peak range, was fitted by five order polynomial to provide adequate description the background in all energy range. The final missing energy spectra, after the fitted background subtraction, are shown in Figs.13-15 (right). One can see clear peak corresponding to the $d(\gamma, p)n$ reaction at the $E_{mis} \approx 2.2$ MeV and, practically, full cancellation the peak of the $^{12}C(\gamma, p)^{11}B_{01}$ reactions, giving confidence in the background subtraction. Looking at the deuteron missing energy peak, a full width at half maximum of about ~ 3 MeV (FWHM) is observed. The dominating contribution to the FWHM width comes from the kinematical spread due to photon energy interval, large angular acceptance of the CsI/SSD telescope and inherent CsI detector resolution.

The reaction yield, Y_{pd}, was obtained from the final $d(\gamma, p)n$ MisE spectra, Figs.13-18 (right), using

two ways:

(i) The $d(\gamma, p)$ peak was fitted by Gaussian,

$$Y = y_0 + \frac{A}{\sigma\sqrt{2\pi}}e^{-\frac{(x-\mu)^2}{2\sigma^2}}, \qquad (9)$$

where the peak position μ, width of the maximum σ, and constant y_0 are the fitting parameters. The reaction yield is determined by relation

$$Y_{pd} = \frac{A}{w}, \qquad (10)$$

where $A = \sqrt{2\pi}\sigma Y_m$ is the square of the fitted Gaussian, Y_m is the Gaussian maximum height, and $w = 0.3$ MeV is the width of the step in the MisE spectrum construction.

(ii) The yield was also obtained by summation the counts in the peak regions, $\mu \pm 3\sigma$. The parameters μ and σ were taken from the Gauss fit. Both methods gave practically the same results of the yields, differing no more 5%. The statistical error of the yields is given by

$$\Delta Y_{pd} \approx \sqrt{N_{CD} + N_{CH} + N_{fit}}, \qquad (11)$$

where N_{CD}, N_{CH} and N_{fit} are the number of counts in the peak-region, $\mu \pm 3\sigma$, for the CD_2 and the CH_2 missing energy spectra and the fitted background spectra, respectively. The background terms N_{fit} is small, $\sim 10\%$ of the sum $N_{CD} + N_{CH}$, thus $\Delta Y_{pd} \approx \sqrt{N_{CD} + N_{CH}}$.

3.5.2. $^{12}C(\gamma, p_{01})^{11}B$ reaction. The random background subtraction

Information on carbon disintegration processes have been obtained from measurements on both targets. The targets provide identical conditions for data taking with exception the low energy bins, $E_{\gamma,bin} < 49$ MeV, in which the peaks of the reactions $^{12}C(\gamma, p_{01})^{11}B$ in missing energy spectra shifted to the range of the deuteron peak, and correct determination of the reaction yield from the CD_2 target data is imposable. As was shown above, the maxima corresponding to the carbon disintegration are on

top of smooth random background, Figs.16-18 (left), which strongly increases with Emis energy increasing. For the background subtraction, special background spectra were generated for every energy bin, taking events from the random range of the corresponding FPtdc spectra, shown in Fig.4. They were normal- ized to the prompt E_{mis} spectra by requiring the same number of the events for the prompt N_{pt} and the random N_r spectra in the selected interval of the background range on the left side of the spectra be- fore the range of the maximum of the $^{12}C(\gamma, p_{01})^{11}B$ reactions.
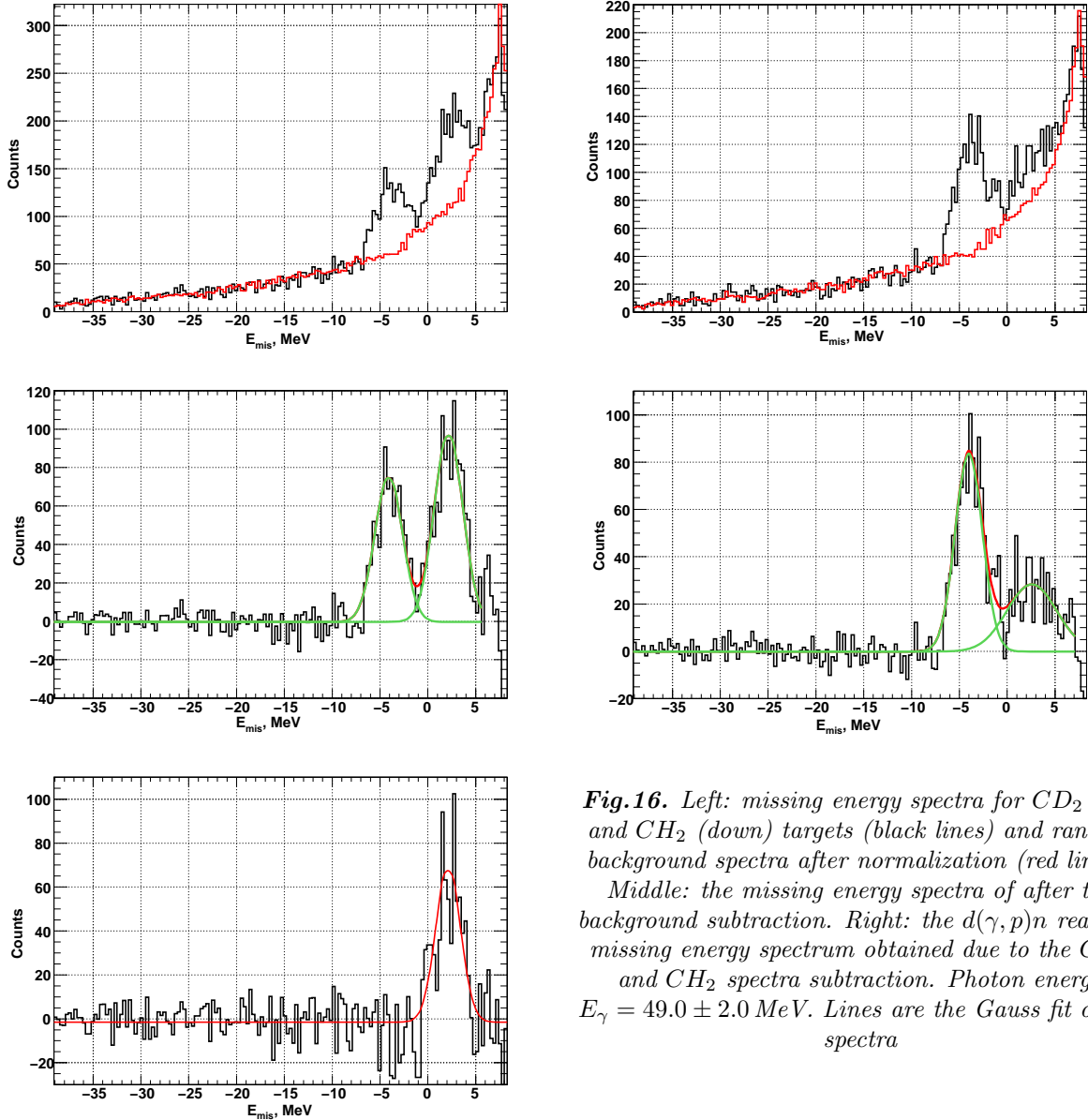
Fig.16. *Left: missing energy spectra for CD_2 (up) and CH_2 (down) targets (black lines) and random background spectra after normalization (red lines). Middle: the missing energy spectra of after the background subtraction. Right: the $d(\gamma, p)n$ reaction missing energy spectrum obtained due to the CD_2 and CH_2 spectra subtraction. Photon energy $E_\gamma = 49.0 \pm 2.0\, MeV$. Lines are the Gauss fit of the spectra*

The normalization coefficient value was deter- mined as,

$$k_{bg} = \frac{N_{pt}}{N_r}. \qquad (12)$$

The k_{bg} values are ~ 0.1 for all energy bins due to wider intervals of the FPtdc spectra which are used for the background missing energy spectra genera- tion, than for the prompt spectra. The normalized background spectra well agree with the prompt ones in the background range, Figs.16-18 (left). Thus af- ter the background subtraction, the spectra both for the CD_2 and CH_2 targets were flat within the sta- tistical errors and consistent with zero in the back- ground range, Figs.16-18 (middle), giving confidence in the background subtraction. On the next step the above CD_2 and CH_2 spectra were subtracted, and the $d(\gamma, p)$ reaction E_{mis} spectra (variant B) were obtained, Figs.16-18 (right). Both variants gave co- incident values of the $d(\gamma, p)$ reaction yield within the statistical accuracy.

Due to decreasing accuracy of the normalization coefficient determination with photon energy increas- ing, resulted from decreasing both level of the back- ground of the prompt spectra in the background range and the background range decreasing (normal- ization interval), as well, an additional control of the background subtraction was applied at data process- ing for energy bins $E_{\gamma, bin} \geq 56.5\, MeV$, using the miss-

ing energy interval of the spectra behind the deuteron peak which becomes enough broad for these energies. The spectra in this interval for the CD_2 and CH_2 targets are determined by the same processes of the carbon disintegration, thus after the background subtraction they have to be, in principle, identical within the statistical accuracy. So, the additional control consisted in requiring the same number of the events for the CD_2 and CH_2 E_{mis} spectra in the selected interval above the $d(\gamma,p)$ peak after the background subtraction. As a rule, the determined k_{bg} values provided also and this control requirement, and after the CD_2 and CH_2 E_{mis} spectra subtration, the $d(\gamma,p)$ spectra were obtained with flat parts, consistent with zero within the statistical errors, below and above the $d(\gamma,p)$ maximum, as shown in Figs.17,18 (right).
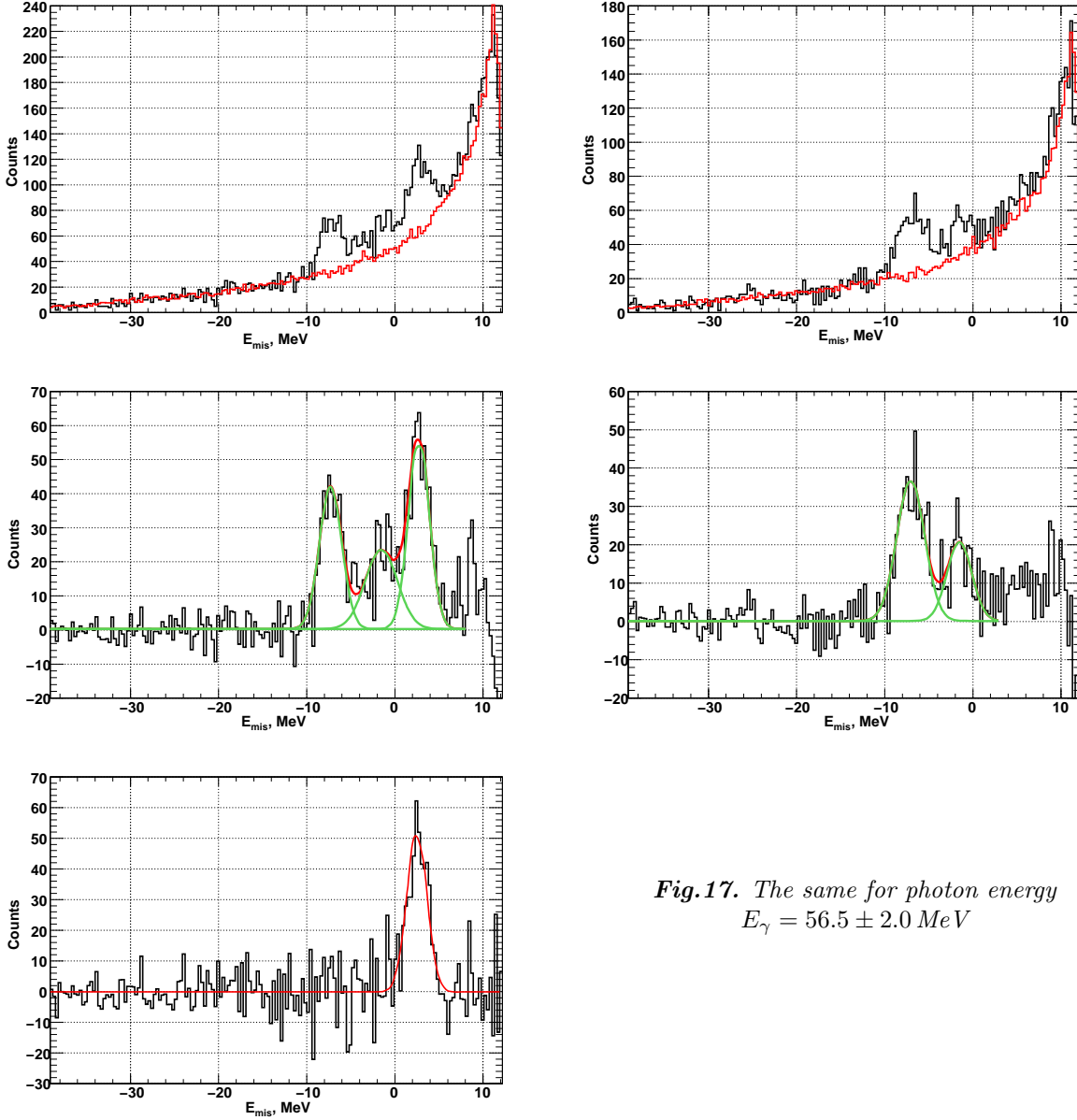
Fig. 17. *The same for photon energy $E_\gamma = 56.5 \pm 2.0\,MeV$*

The yield of the $d(\gamma,p)n$ reaction for the variant B data processing was obtained by the same way, as for the previous variant A, using both the Gauss fit of the peak and summation events under the peak. The statistical errors of the yield for variant B are calculated by

$$\Delta Y_{pd} = \sqrt{N_{CD_2} + k_{bgCD_2}^2 N_{BgCD_2} + N_{CH_2} + k_{bgCH_2}^2 N_{BgCH_2}}\,, \qquad (13)$$

where N_{BgCD_2} and N_{BgCH_2} are the number of counts in the peak region, $\mu \pm 3\sigma$, for the background the CD_2 and CH_2 missing energy spectra, respectively. Because normalization coefficient is $k_{bg} \sim 0.1$, contribution of the background terms is small, $\sim 10\%$, and the statistical errors were determined by statistics of the prompt peak yields for the CD_2 and CH_2 targets, $\Delta Y_{pd} \approx \sqrt{N_{CD_2} + N_{CH_2}}$, as for the variant A. The statistical accuracy of the yields varied from $\sim 10\%$ at $E_\gamma = 41.2\,\text{MeV}$ bin to $\sim 15\%$ for $E_\gamma = 70.8\,\text{MeV}$.

The results of the A and B variants of the data processing within the data accuracy practically coincide for all photon energy bins that also gave confidence of the $^{12}C(\gamma,p_{01})^{11}B$ reaction yield obtaining.
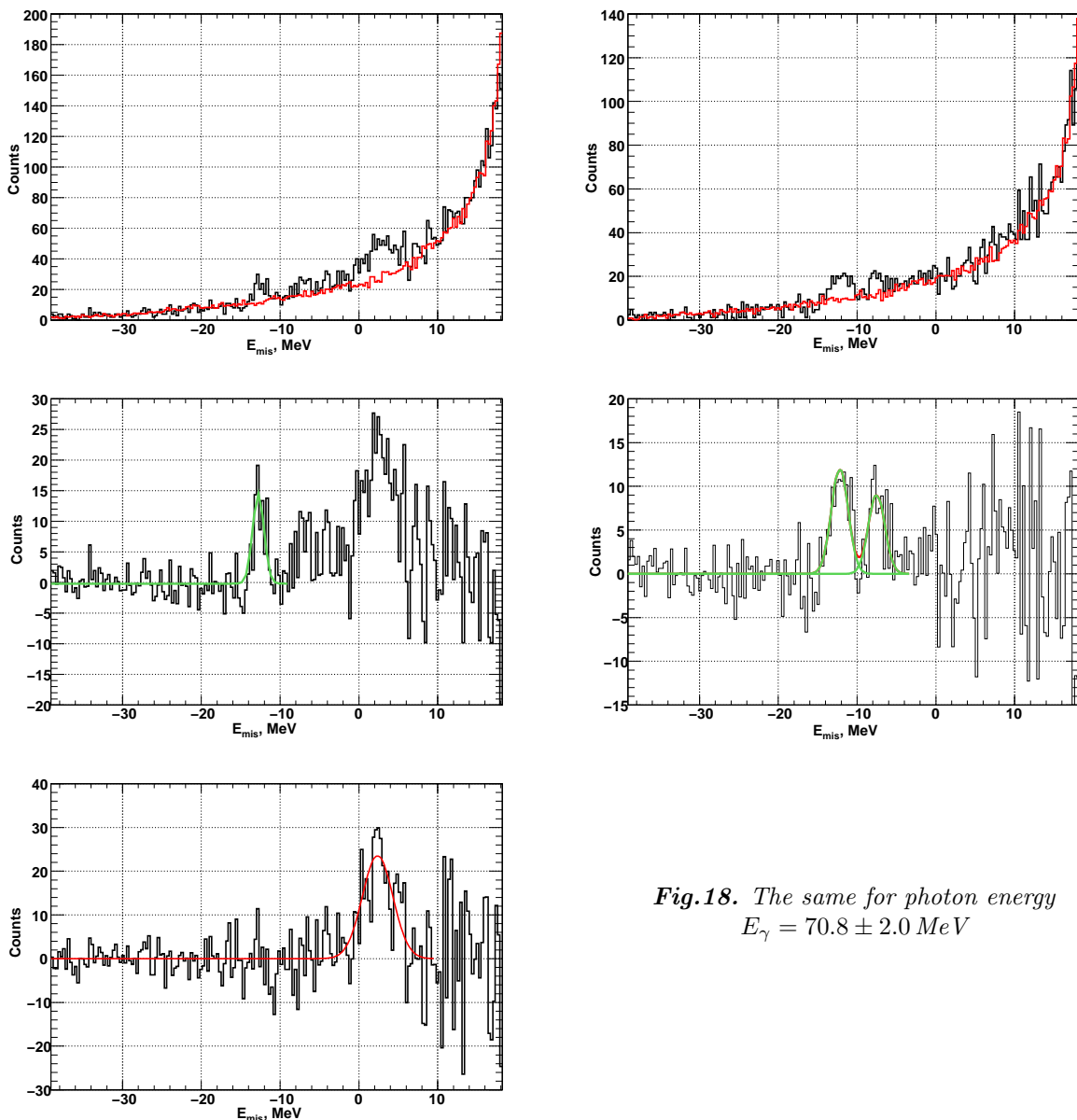
Fig.18. *The same for photon energy*
$E_\gamma = 70.8 \pm 2.0\,MeV$

The yields of the carbon disintegration were obtained by the same way, both Gauss fit and summation the events under $^{12}C(\gamma,p_{01})^{11}B$ peak. At some photon energies we used two Gaussians for correct separation the contributions resulted from the higher exited states or the deuteron disintegration process to the peak of the $^{12}C(\gamma,p_{01})^{11}B$ reaction. The Gauss fit and summation gave the same results within the statistical accuracy. The statistical error of the reaction yields is given by

$$\Delta Y_{CD(CH)} = \sqrt{N_{CD(CH)} + k_{bg}^2 N_{BgCD(CH)}}, \quad (14)$$

where $N_{CD(CH)}$ and $N_{BgCD(CH)}$ are the number of counts in the peak region, $\mu \pm 3\sigma$, for the CD_2 (or CH_2) prompt and background missing energy spectra, respectively. Because, as stated the above, the normalization coefficient is $k_{bg} \sim 0.1$, contribution the second term is $\sim 10\%$ and the statistical errors were determined mostly by statistics of the prompt peak, $\Delta Y_C \approx \sqrt{N_{CD(CH)}}$. The statistical accuracy of the yields for both targets varied from $\sim 3\%$ at $E_\gamma \sim 40\,MeV$ to $\sim 20\%$ for end of the tagging interval $E_\gamma \sim 70\,MeV$ due to strong decreasing of the $^{12}C(\gamma,p_{01})^{11}B$ reaction cross section.

3.5.3. Cross section

The cross section was calculated using the formula

$$\frac{d\sigma}{d\Omega} = \frac{Y_{p,i}}{N_{D(C)}\Delta\Omega N_\gamma(i)\varepsilon_{st,i}}, \quad (15)$$

where

- $Y_{p,i}$ is the reaction yield for i-th energy bin;
- $N_{D(C)}$ is the number of deuterons (carbons) nuclei per cm^2 for the target located under angle $\theta_m = 60^0$ to the photon beam direction. They are

61

for deuteron $N_D = 1.541 \times 10^{22} D/cm^2$, and for carbon $N_{C(CD_2)} = 0.771 \times 10^{22} C/cm^2$ for the CD_2 and $N_{C(CH_2)} = 0.885 \times 10^{22} C/cm^2$ for the CH_2 target.

- $\Delta\Omega = 249.00 \pm 2.25\,msr$ is the effective solid angle of the CsI/SSD telescope;

- $N_\gamma(i) = N_{FP}(i)\varepsilon_{tag}(i)$ is the tagged photon flux incident on the target. $N_{FP}(i)$ is the number of post-bremsstrahlung electrons, corresponding to the i-th energy bin, $\varepsilon_{tag}(i)$ is the tagging efficiency. We use the experimental value of the tagging efficiency, averaged over tagged energy range, $\varepsilon_{tag}(i) = 0.35$;

- $\varepsilon_{st,i}$ is the stolen correction to the cross section for the for the i-th energy bin. This correction resulted from the fact that the uncorrelated electron can be registered in the region to the left of the prompt peak, thus a focal plane TDC can be stopped by a random electron, arriving earlier than a correlated. If the random events are Poisson-distributed in time, the stolen-coincidence correction may be written as [8],

$$\varepsilon_{st,i} = e^{-\frac{t_0 n_{FP,i}}{df}}, \qquad (16)$$

where $n_{FP,i}$ is the efficient rate of the FP counters, corresponding to the i-th energy bin, t_0 is the position of the lower limit of the prompt region in the FPtdc spectrum, df is the average duty factor of the beam during the run. The stolen correction is proportional to the count rate in the focal-plane detectors and inversely proportional to the duty factor. The rate of the focal plane detectors corresponding to the i-th energy bin is ranged from $n_{FP,i} \sim 0.4$ to $1.2\,MHz$. The prompt peak position was in the 750 channel for all FPtdc spectra, the lower limit of the prompt region was taken at 727 channel that corresponded to $t_0 \approx 128\,ns$. The average value of the duty factor over all beam runs was $df = 0.5$. The average FP counting rate n_{FP} for CD_2 and CH_2 runs differed no more 10%, thus the stolen-coincidence corrections were practically identical for both runs and varied with energy from $\varepsilon_{st,i} \sim 24\%$, at $E_\gamma = 41.2\,MeV$, to $\varepsilon_{st,i} \sim 11\%$ at $E_\gamma = 78\,MeV$.

The differential cross sections of the $d(\gamma,p)n$ reaction obtained for variants A and B of the data processing are shown in Fig.19. They are in agreement within the data accuracy with each other and with the data of other laboratories. However, if to consider ratio of the cross section, obtained for A and B variants of the data processing, averaged over whole energy interval of the measurements, there is a systematic $\sim 10\%$ exceeding of the cross sections for variant A above the data for variant B. This value can be considered as systematic error of the measured cross section.

The differential cross sections of the $^{12}C(\gamma,p_{01})^{11}B$ reaction are shown in Fig.20. As can be seen, the data obtained from measurements on the CD_2 and CH_2 targets are in a good agreement within the data accuracy.
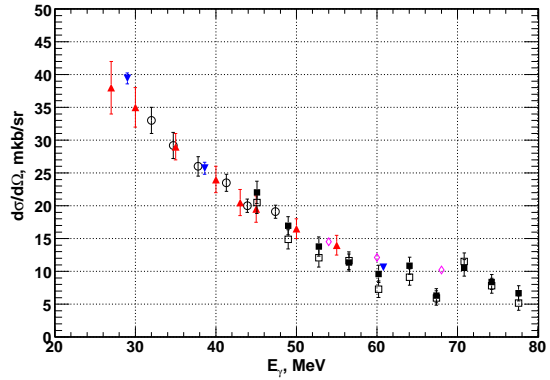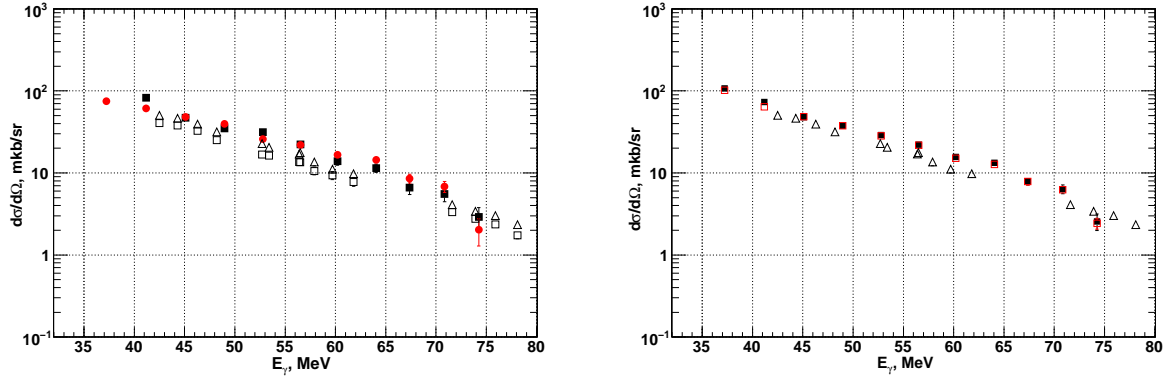

Fig.19. *Differential cross section of the $d(\gamma,p)n$ reaction at $\theta_p = 90^0$ for variants A (full squares) and B (empty squares) data processing. The literature data: [9] (circles), [10] (rhombus), [11] (down triangles), [12] (triangles)*

The ratio of the cross sections average over energy interval of the measurements is $R = 1.03 \pm 0.08$ for yields obtained by summation and $R = 0.97 \pm 0.06$ for yields obtained by Gauss fit. The average differential cross sections over these runs are shown in Fig.20 (right). Due to large angular capture of the telescope and strong angular dependence of the cross section, the effective angle of the proton detection was less the geometrical angle of the telescope position relatively the photon beam. It was calculated using the cross section angular dependences from [1]. The obtained effective angle values were $\sim 3^0$ till $\sim 5^0$ less the angle of the telescope position (90^0) at photon energy increasing from $E_\gamma \sim 40\,MeV$ to $\sim 62\,MeV$. Such change of the proton emission angle increases the cross section from 10% to 30% in this energy interval, respectively. If to take into account the effective angle of the proton registration, our data are in a reasonable agreement with the data [1], presented in the Fig.19 for angle of the proton emission $\theta_p = 90^0$.

4. SUMMARY

The $\Delta E - E$ CsI/SSD telescope, constructed in MAX-lab, has been tested, in order to evaluate its characteristics and capabilities for measurements the (γ, p) reactions on atomic nuclei at intermediate energies, ranging from the Giant Dipole Resonance and up to several tens of MeV below threshold for pion photoproduction. The telescope consists of two single-sided silicon strip detectors, with effective strip width 2 mm, and CsI counter which function as (ΔE) and (E) detectors, respectively. The Monte Carlo simulation of the experimental set up have been performed, including generation of the photon beam and passing it to the target through a collimator, the beam tagging efficiency and the telescope angular capture and the effective solid angle value.

Fig.20. *Left: The differential cross section for the $^{12}C(\gamma, p_{01})^{11}B$ obtained from the CD_2 (squares) and CH_2 (circles) runs. Right: the cross section averaged over CD_2 and CH_2 runs obtained by summation (full squares) and Gauss fit (empty squares) of the reaction missing energy peak. Triangles are the data [1] for $\theta_p = 90^0$*

The simulation has shown that the existing construction of the telescope provided rather large geometrical angular capture $\Delta\theta_p \approx 30^0$ (FWHM) if do not use the triggered strip information from the SSD detectors. The angular resolution can be improved by factor of two if to select the particles trajectories, passing through the strips with identical numbers.

The possibility of $\Delta E - E$ method of proton identification and the (γ, p) reaction selection by the missing energy method were studied using reactions of a deuteron and a carbon disintegration. The energy calibration of the CsI detector was performed which has demonstrated a linear dependence between the energy of incoming proton and the CsI signal within energy interval $T_p = 10...50\,MeV$, and threshold of the proton registration $T_p \approx 18\,MeV$. So, the CsI/SSD telescope at present construction provides measurements of the (γ, p) reactions on atomic nuclei in photon energy range $E_\gamma > 40\,MeV$, where quasi-deuteron mechanism of the nuclear disintegration is important. For testing the missing energy method for the reaction selection and background subtraction, cross sections of the $d(\gamma, p)n$ and the $^{12}C(\gamma, p_{01})^{11}B$ reactions were measured in the range $E_\gamma \approx 40...70\,MeV$, which agreed with literature data. In order to extend investigations in the Giant Dipole Resonance region it is necessary to decrease the threshold of the proton registration, using thinner coordinate detectors and nuclear targets, and placing telescope into special vacuum chamber. It will allow one to improve energy resolution and resolve the exited state of the final of nucleus. The angular resolution of the telescope can be improved if to use coordinate information on the triggered strips of the silicon strip detectors.

The obtained results give the possibility, using the existing at MAX-lab technique, to extend the (γ, p) processes investigation involving the polarized photon beam, produced at MAX-lab. Such experiments will allow one to get new physical observation and open new possibility for investigation of nuclear structure and photonuclear reaction mech-

anisms in this energy range. Analysis of results of the $^{12}C(\gamma, p_{01})^{11}B$ reaction measurements with the polarized photon beam will be presented in the next paper.

References

1. H. Ruijter et al. Angular distribution for the $^{12}C(\gamma, p)^{11}B$ reaction // *Phys.Rev. C54. 1996, p.3076.*

2. V. Ganenko et al. Linearly polarized photon beam at MAX-lab // *Nuclear Inst. and Methods in Physics Research, A. 2014, p.137-149.*

3. S. Al. Jebali, et al. Summary of the MAX-lab Run Period 2008.02.18 - 2008.03.17

4. J.-O. Adler et al. The upgraded photon tagging facility at MAX-lab // *Nucl. Instr. and Meth. A715, 2013, p.1-10.*

5. J. Brudvik, et al. Summary of the MAX-lab Run Period 2008.04.14 - 2008.04.28

6. E. Aghassi, et al. Summary of the MAX-lab Run Period 2008.06.02 - 2008.06.30

7. http://geant4.cern.ch

8. R.O.Owens // *Nucl. Instrum. and Methods.* 1990, A288, p.574.

9. D. Babusci, V. Bellini, M. Capogni, et al. Deuteron photo-disintegration with polarized photons in the energy range 30-50 MeV // *Nucl. Phys.* 1998, A633, p.683-694.

10. K.-H. Krause, J. Sobolewski, J. Ahrens, et al. Photodisintegration of the deuteron by linearly polarized photons // *Nucl. Phys.* 1992, A 549, p.387-406.

11. M.P. De Pascale, G. Giordano, G. Matone, et al. // *Phys. Rev.* 1985, C 32, p.1830

12. B. Weissman and H.L. Schultz // *Nucl.Phys.* 1971, A 174, p.129.

ИЗМЕРЕНИЕ (γ, p) - РЕАКЦИЙ НА УСТАНОВКЕ MAX-лаб С ПОМОЩЬЮ ΔЕ-Е ТЕЛЕСКОПА

Д.Д. Бурдейный, J. Brudvik, В.Б. Ганенко, K. Hansen, K. Fissum, L. Isaksson, K. Livingston, M. Lundin, B. Nilsson, B. Schröder

Рассматриваются результаты экспериментов по изучению реакций $^{12}C(\gamma,p)^{11}B$ и $d(\gamma,p)n$ в области энергий меченых фотонов 35...80 МэВ. Показана возможность идентификации протонов методом ΔЕ-Е с помощью CsI/SSD - телескопа. Используя спектры недостающих энергий, определены значения дифференциальных сечений рассматриваемых реакций в указанных диапазонах энергий фотонов. Показано хорошее согласие результатов экспериментов с имеющимися литературными данными.

ВИМІРЮВАННЯ (γ, p) - РЕАКЦІЙ НА УСТАНОВЦІ MAX-лаб ЗА ДОПОМОГОЮ ΔЕ-Е ТЕЛЕСКОПА

Д.Д. Бурдейний, J. Brudvik, В.Б. Ганенко, K. Hansen, K. Fissum, L. Isaksson, K. Livingston, M. Lundin, B. Nilsson, B. Schröder

Розглянуто результати експериментів з вивчення реакцій $^{12}C(\gamma,p)^{11}B$ і $d(\gamma,p)n$ в області енергій мічених фотонів 35...80 MeB. Показана можливість ідентифікації протонів методом ΔЕ-Е за допомогою CsI/SSD - телескопа. Використовуючи спектри недостатніх енергій визначені диференційні перерізи розглянутих реакцій в зазначених діапазонах енергій фотонів. Отримані експериментальні результати добре узгоджуються із літературними даними.